Heliyon 10 (2024) e37583

Contents lists available at ScienceDirect

Heliyon

journal homepage: www.cell.com/heliyon

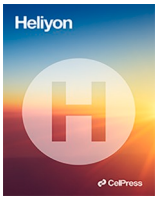

Research article

Association of bacteriomes with drug susceptibility in lesions of pulmonary tuberculosis patients

Weili Du, Yingli Zhao, Chen Zhang, Li Zhang, Lijuan Zhou, Zuyu Sun, Xiaojie Huang, Nana Zhang, Zichen Liu, Kun Li, Nanying Che *

Department of Pathology, Beijing Key Laboratory for Drug Resistant Tuberculosis Research, Beijing Chest Hospital, Capital Medical University, Beijing Tuberculosis and Thoracic Tumor Research Institute, Beiguandajie 9#, Tongzhou Dist, Beijing, 101149, China

ARTICLE INFO

Keywords:
Pulmonary bacteriomes
TB lesions
Drug susceptibility
Bacterial metabolic functions

ABSTRACT

Understanding how the bacteriomes in tuberculous lesions can be influenced by the susceptibility of *Mycobacterium tuberculosis* (MTB) can provide valuable information for preventing and treating drug resistant tuberculosis (DR-TB). High-throughput 16S rRNA sequencing was employed to analyze the bacteriome in pulmonary TB lesions from 14 patients with DR-TB and 47 patients with drug sensitive tuberculosis (DS-TB), along with 18 normal lung tissues (NT) from 18 lung cancer patients serving as the bacterial baseline. The phylogenetic investigation of communities by reconstruction of unobserved states2 (PICRUSt2) algorithm was utilized to predict bacterial metabolic functions. The major phyla of pulmonary bacteriomes included *Proteobacteria*, *Actinobacteria*, *Bacteroidetes*, *Firmicutes* and *Fusobacteria*. Alpha diversity indices, including ACE, Chao1, Shannon and OTU observed, all demonstrated different bacterial communities of DS-TB samples from that of NT samples; while only Shannon indicated difference between DR-TB and NT samples. The analysis of similarity (ANOSIM) showed significantly different bacterial communities within TB lesions compared to NT samples ($R = 0.418$, $p = 0.001$). However, difference was not observed between DR-TB and DS-TB samples (ANOSIM, $R = 0.069$, $p = 0.173$). The bacterial profiles within each DR-TB individual appeared unique, with no obvious clusters corresponding to drug-resistant phenotypes. Nevertheless, indicator genera identified in DR-TB and DS-TB lesions demonstrated distinctive micro-ecological environments. Most COG functions were enriched in TB lesions, and the most significant one was [J] translation, ribosomal structure and biogenesis. The distinct enrichment patterns of bacterial enzymes in DR-TB and DS-TB lesions suggest that pulmonary bacterial activities can be modulated by the susceptibility of MTB bacilli. This study provides fresh perspectives and strategies for the precise diagnosis and assessment of drug resistance tuberculosis.

1. Introduction

Drug-resistant pulmonary tuberculosis (DR-TB) results from *Mycobacterium tuberculosis* (MTB) strains that exhibit resistance to first- and/or second-line anti-tuberculosis medications, often due to inappropriate antibiotic treatment or irregular drug intake [1]. The mechanisms underlying resistance to anti-tuberculosis drugs are intricate, primarily involving special cell wall structures, drug efflux

* Corresponding author. Department of Pathology, Beijing Chest Hospital, Beiguandajie 9#, Tongzhou Dist, Beijing, 101149, China.
E-mail address: chenanying@bjxkyy.cn (N. Che).

https://doi.org/10.1016/j.heliyon.2024.e37583
Received 24 April 2024; Received in revised form 3 September 2024; Accepted 5 September 2024
Available online 6 September 2024

pump systems, cell metabolism and genetic mutations [2]. According to the World Health Organization (WHO), approximately 10.6 million people were infected with MTB in 2021. Among them, 410,000 cases were classified as rifampicin-resistant or multidrug-resistant TB (RR/MDR-TB) [3]. Due to the rapid advancements in DR-TB diagnostic techniques [2,4], approximately half a million new cases of RR/MDR-TB are reported annually, yet only one-third of these cases receive appropriate treatment [3]. The spread of DR-TB significantly undermines the global goals set by the End TB Strategy and is a major global health concern, particularly in low-income regions and countries [5]. Interactions between the host immune system and MTB is the crucial role in determining the outcome of DR-TB after anti-tuberculosis drug treatment [6], while host microbiome is another factor that cannot be ignored in the development of tuberculosis.

Growing researches highlight the associations between the host microbiome and MTB initial colonization, anti-tuberculosis immune responses, prevention and therapy [7]. The gut microbiota, a complex and dynamic ecosystem housing approximately 100 trillion commensal microorganisms can modulate pulmonary immune status by secreting metabolites and other mediators, creating what is known as the "gut-lung axis" [8,9]. Specific anaerobic bacteria are enriched in the gut microbiota of pulmonary TB patients and can predict upregulation of pro-inflammatory immunological pathways [10]. Additionally, a commensal gut bacteria-regulated long non-coding RNA (lncRNA) was found to be down-regulated due to gut microbiota dysbiosis caused by MTB infection, which interacts with enhancer of zeste homolog 2 (EZH2), leading to enhanced IFN-γexpression [11]. In DR-TB patients, coliform flora in the gut is significantly enriched and associated with fatty acid synthesis in the blood [12]. Overall, the gut microbiota plays a critical role in regulating pulmonary TB.

The lungs are also colonized by organisms [13,14]. After MTB infection, the genera such as *Rothia*, *Leuconostoc* and *Lactobacillus* were mostly prevailed in sputum compared to normal control groups [15]. Sputum microbiota has been proposed as a potential diagnostic marker for mono- or multidrug-resistant TB [16,17]. Besides sputum samples, bronchoalveolar lavage (BAL) and throat swabs also showed altered lung bacterial diversity after MTB infection, but the altered bacterial profiles are inconsistent [18,19]. Sputum, BAL and throat swabs are respectively collected from the lower respiratory tract, lung, and the upper respiratory tract. The inconsistency of the reported results of lung bacteriomes may be due to the different collection sites. Importantly, the bacterial load in lung tissue is two orders of magnitude higher than in the aforementioned samples, making lung tissue the preferred specimen type for studying lung microbiota [20]. Organized granulomas are typical lesions in pulmonary TB, where MTB persists and anti-tuberculosis immune responses occur [21]. Therefore, the microbiome within granulomas should deserve more attention when assessing the impact of lung microbiota on pulmonary TB.

Drug-resistant genetic mutations have been found to confer different fitness costs for MTB [22]. A study also indicates that MTB carrying a rifampicin drug resistance mutation can influence macrophage metabolic reprogramming through altering the expression of its surface lipids [23]. We hypothesize that there may be associations between lung bacteriomes and TB drug resistance. Elaborating the effect of lung bacteriome and their metabolic activities on pulmonary TB is essential for advancing future strategies in preventing and treating drug-resistant TB.

The human inherent microbiota interacts with the human host and the environment through their metabolic activities. Bacterial metabolic functions are even more critical for the ecosystem than just taxonomic composition, while bacterial metabolic functions are often decoupled from taxonomic composition [24]. To address this issue, the algorithm Phylogenetic Investigation of Communities by Reconstruction of Unobserved states2 (PICRUSt2) has been developed [25]. PICRUSt2 predicts bacterial metabolic functions using 16S rRNA high-throughput sequencing data, and its performance is comparable to whole-genome sequencing, leading to its widespread application.

In this study, we collected lung tissues from pulmonary TB and lung cancer patients who had undergone surgical treatment. Based on phenotypic drug susceptibility test (pDST) results, TB lesions were categorized into drug-resistant tuberculosis (DR-TB) and drug-sensitive tuberculosis (DS-TB). Bacteriome characteristics in TB lesions were investigated using normal lung tissues as bacterial baseline by 16S rRNA sequencing method. Bacterial metabolic functions in lung tissues were also predicted using the PICRUSt2 algorithm to explore potential interactions between pulmonary bacteria and drug susceptibility.

Table 1
Characteristics of drug resistant and drug sensitive pulmonary TB patients.

Variable	TB Culture Result, No. (%)	
	Drug resistant (n=14)	Drug sensitive (n=47)
Age, average (std)	45.0 ±13.6	41.6 ± 14.8
Male	8 (57.1)	29 (61.7)
Any cancer	0 (0)	1 (2.1)
Cough	5 (35.7)	22 (46.8)
Sputum production	4 (28.6)	15 (31.2)
Hemoptysis	3 (21.4)	8 (17.0)
Fever	3 (21.4)	10 (21.3)
Night sweats	1 (7.1)	8 (17.0)
Weight loss	2 (14.3)	8 (17.0)
Tissue AFB positive	8 (57.1)	29 (61.7)
Cavitation on chest CT	4 (28.6)	15 (31.9)

2. Materials and methods

2.1. Clinical characterization of the participants

Retrospectively, 63 formalin fixed and paraffin embedded (FFPE) TB lesions were obtained from 63 pulmonary TB patients who had undergone surgical treatment at the Department of Pathology, Beijing Chest Hospital between January 2020 and December 2020 (Table 1). The diagnostic criteria for pulmonary TB met either of the following conditions: 1) positive mycobacterial culture for sputum or BAL, or 2) positive TB-PCR targeting the *IS6110* fragment specific to TB lesions. All patients included in the study were culture-positive, and phenotypic drug susceptibility testing (pDST) was conducted using a commercial 96-well plate containing lyophilized antibiotics according to manufacturer's instructions (Encode Medical Engineering Co, Zhuhai, China). Patients were categorized as 14 DR-TB because their pDST results indicated resistance to at least one drug; and 47 DS-TB because their pDST results indicated drug sensitive. Among the 14 DR-TB patients, they can be classified as follows: 2 for rifampicin resistant, 3 for isoniazid resistant, 2 for fluoroquinolone resistant, 1 for rifampicin-isoniazid resistant, 1 for rifampicin-isoniazid-ethambutol resistant, 1 for rifampicin-isoniazid-fluoroquinolone resistant, and 4 for rifampicin-isoniazid- fluoroquinolone-ethambutol resistant. The percentages of DR-TB patients manifesting symptoms such as cough, hemoptysis, fever, night sweets, weight loss and cavitation on chest CT were not statistically different from those of DS-TB patients. The acid-fast bacilli (AFB) positive ratio in DR-TB and DS-TB lesion tissues were 57.1 % (8/14) and 61.7 % (29/47), respectively. Additionally, 18 normal lung tissues (NT), located more than 2 cm distal to tumor lesions in lung cancer patients who had undergone surgical treatment, were obtained to serve as the bacterial baseline. None of the participants had taken any medications for human immunodeficiency disease prior to sample collection.

2.2. DNA extraction and processing

Normal lung tissues surrounding the TB lesions were excised from the FFPE samples following hematoxylin-eosin (HE) staining, retaining 0.5–1.0 cm^2 lesion areas. These HE-stained lesion areas exhibited necrotic or non-necrotic granulomatous inflammation with visible epithelial cells, chronic inflammatory cells, and/or Langhans giant cells, all enriched by fibrous connective tissue. The NT samples with 0.5–1.0 cm^2 areas were selected, and the HE-stained NT samples displayed a normal lung lobule structure. Twenty sections (4 μm) of TB lesions or NT samples were utilized for DNA extraction with the QIAamp DNA FFPE Tissue Kit 56,404 (QIAGEN, Hilden, Germany), following the manufacturer's instructions. DNA concentration was quantified using a NanoDrop 2000 spectrometer (Thermo Fisher Scientific, Waltham, United States). DNA integrity was assessed via 1 % agarose gel electrophoresis.

Amplification of 16S rRNA V4 hypervariable regions was performed using primer sets, 515F/806R, which included barcodes at the 5' end of the forward primers [26]. The PCR reaction system consisted of 50 μL, with 2 μL primer sets (10 μmol/L), 25 μL 2 × KAPA HiFi HotStart ReadyMix (Kapa Biosystems, MA, United States) and 23 μL extracted FFPE DNA. The PCR protocol included: initial denaturation at 95 °C for 3 min, 30 cycles of denaturation (20 s at 98 °C), annealing (15 s at 55 °C) and extension (15 s at 72 °C), with a final extension step at 72 °C for 10 min. The PCR reaction was performed in triplicate for each sample. Subsequently, the three PCR products were pooled together and purified through 2 % agarose gel electrophoresis. An agilent 2100 bioanalyzer (Agilent Technologies, Palo Alto, California) was utilized to confirm the fragment size and distribution of the constructed DNA library. Finally, the library was barcode indexed with the NEB Next Ultra DNA Library Prep Kit for Illumina (New England Biolabs, United States) and sequenced on an Illumina MiSeq PE 250 machine.

2.3. 16S rRNA gene analysis

The raw 16S rRNA sequencing data were analyzed using QIIME v1.9 [27]. The sequences were quality trimmed and filtered (fastq_maxee = 0.5) using QIIME default parameters. At 97 % sequence similarity, all qualified sequences were clustered into operational taxonomic unit (OTUs) using the closed-reference OTU picking methods using USEARCH v7.0.1090 [28]. OTUs with a number of sequences less than 0.005 % of the total number of sequences were discarded [29]. Bacterial taxonomic assignment was conducted using Greengenes2. Sequences that mapped to the mitochondrial and chloroplastic genomes were discarded. All samples were rarefied to the same sequence number based on the sample that yield the fewest sequences. The final rarefied OTU table, containing the abundances of bacterial taxa in each sample, was used for downstream analyses. A-diversity indexes, including Chao1 richness, Shannon diversity, and Good's coverage, as well as the β-diversity index (Bray-Curtis distance metrics) were calculated using the QIIME platform. Additionally, bacterial functions were predicted using PICRUSt2 from 16S rRNA sequences [25].

2.4. Statistical analysis

Principal coordinates analysis (PCoA), based on Bray-Curtis distance, was employed to illustrated the characteristics of bacterial diversity among different pulmonary tissue categories. This analysis utilized the "ggplot2" package for R [30]. To statistically validate bacterial clustering in the PCoA analysis, we employed the analysis of similarity (ANOSIM) algorithm. We evaluated significant differences in bacterial richness and diversity using Kruskal-Wallis tests, followed by Dunn's multiple comparison test in the "FSA" packages. Additionally, wilcoxon rank sum test was used to calculate statistical differences between bacterial functions of the two categories. All these analyses were performed using the R software program (v.3.2.1); you can find more information about R at this link: http://www.r-project.org).

3. Results

3.1. Bacterial composition among DR-TB, DS-TB and NT samples

After performing sequence quality control and filtering out DNA fragments related to mitochondria and chloroplast, we obtained a dataset of 16S rRNA gene fragments containing 4,464,966 valid sequences. The sequence numbers for each sample ranged from 33,249 to 64,509. To mitigate bacterial discrepancies caused by varying sequencing depths, all sample sequences were rarefied to 33,249.

At the phylum level, *Proteobacteria*, *Actinobacteria*, *Bacteroidetes*, *Firmicutes* and *Fusobacteria* were major taxa, together accounting for 96.01 % of the total reads (Fig. 1A). The archaeal phylum *Euryarchaeota* was also observed predominantly in both DS-TB and DR-TB lesions. In TB lesions, the relative abundances of *Proteobacteria* ($p = 0.039$), *Actinobacteria* ($p = 0.002$) and *Firmicutes* ($p = 0.028$) were significantly higher compared to NT samples. In the phylogenetic tree analysis of order level, the individual bacterial bacteriome of DR-TB clustered together with those of DS-TB, while the bacterial populations in the NT samples formed two separate branches (Supplemental Fig. 1). At the genus level, dominant taxa in lung tissues included *Bukholderlaceae* spp., *Pseudomonas*, *Mycobacterium*, *Sphingomonas* and *Bacteroides* (Fig. 1B). There was also no significant difference in bacterial taxa between DS-TB and DR-TB groups at the genus level. The relative abundance of the genus *Mycobacterium* in DS-TB samples was slightly higher than that in DR-TB and NT samples, but this difference was not statistically significant (Fig. 1C). In totally, 1173 OTUs were clustered based on the 97 % similarity threshold (Fig. 1D). Among all sample types, 65.8 % of the OTUs were shared (772 out of 1173). Notably, the proportion of specific OTUs in DS-TB samples (8.1 %, 95 out of 1173) was significantly higher than that in DR-TB (0.4 %, 5 out of 1173) and NT (0.3 %, 3 out of 1173) samples.

Indicator genera can serve as signals of distinctive microenvironments within various ecological niches. We conducted an indicator value (IndVal) analysis, considering an indicator value > 0.60 and $p < 0.05$, to identify indicator genera in DS-TB, DR-TB and NT samples (Fig. 2). In DS-TB lesions, there were 7 indicator genera, spanning the phyla *Actinobacteria*, *Bacteroidetes*, *Firmicutes*, *Fusobacteria* and *Proteobacteria*. Notably, an uncultured taxon affiliated with *Actinobacteria* was observed as an indicator genus in the DS-TB group. In both DR-TB and NT samples, the indicator genera belonged to the phylum *Proteobacteria*.

The alpha diversities of the bacteriome in DS-TB, DR-TB and NT were evaluated using ACE, Chao 1, Shannon and OTUs observed (Table 2). Notably, these four bacterial diversity indexes showed that DS-TB lesions were significantly higher than those observed in NT samples. Only Shannon index showed different bacterial diversity between DR-TB and NT samples. There was no statistical difference in alpha diversity between the DS-TB and DR-TB groups. We further conducted a principle coordinates analysis (PCoA) based on bacterial taxa at the OTU level. The results revealed that the bacterial community structure in TB lesions distinctly separated from that of normal samples (Fig. 3A). This separation was further confirmed by the analysis of similarity (ANOSIM) ($R = 0.418$, $p = 0.001$).

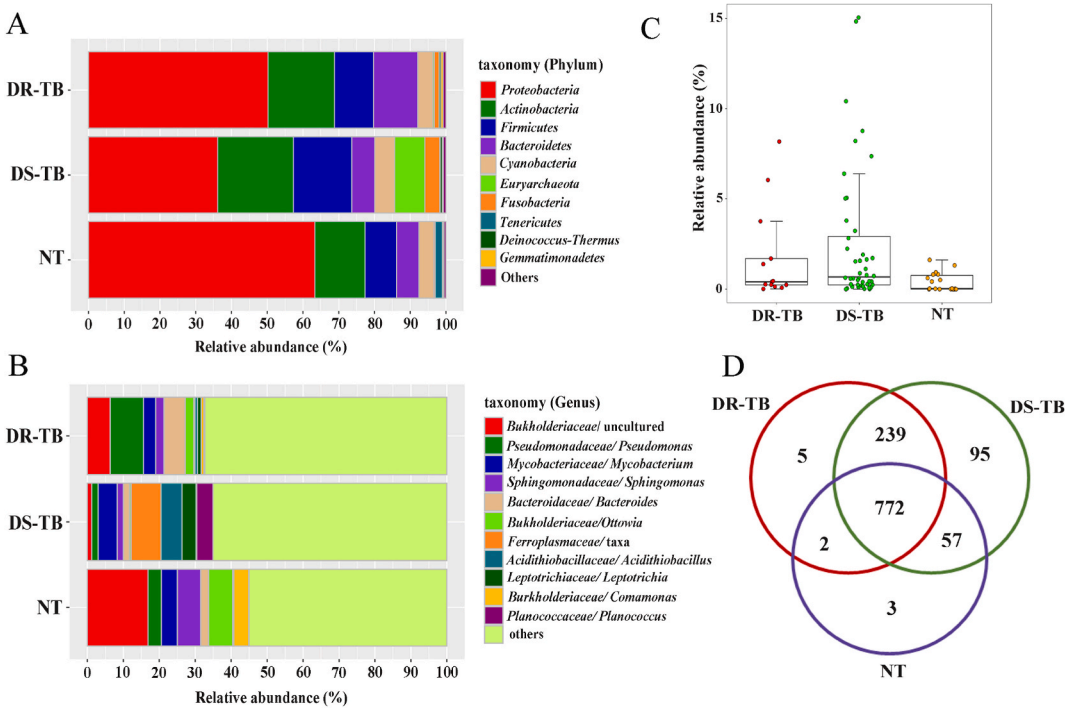

Fig. 1. (A) Average relative abundances of phylum-level taxa showing the distribution of bacterial compositions. (B) Average relative abundances of genus-level taxa showing the distribution of bacterial compositions. (C) Box plot of relative abundance of genus *Mycobacterium*. (D) Venn diagram of the exclusive and shared OTUs. DR-TB: drug resistant tuberculosis; DS-TB: drug sensitive tuberculosis; NT: Normal tissues.

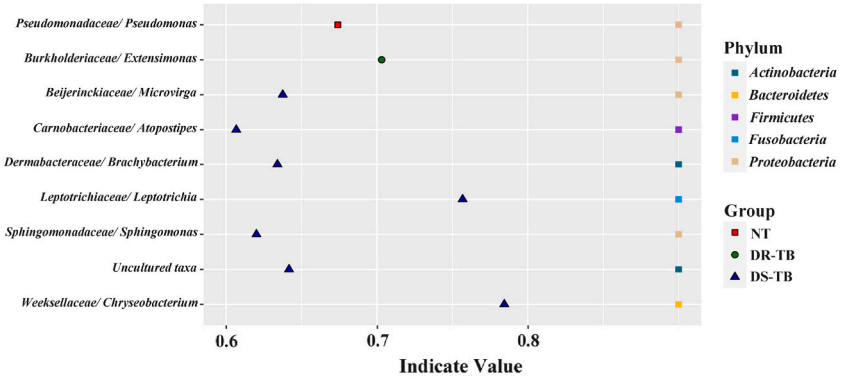

Fig. 2. IndVal analysis showing indicator genera in DR-TB, DS-TB and NT samples. Genera taxa with an indicator value > 0.60 and $p < 0.05$ are identified as indicators. DR-TB: drug resistant tuberculosis; DS-TB: drug sensitive tuberculosis; NT: Normal tissues.

Table 2
Characteristics of bacteria richness and diversity indices.

Categories	ACE	Chao 1	Shannon	OTU observed
DR-TB	349.1 ± 119.7^{ab}	353.0 ± 123.1^{ab}	4.98 ± 1.52^{a}	312 ± 115^{ab}
DS-TB	407.3 ± 73.7^{a}	410.4 ± 77.3^{a}	5.41 ± 1.12^{a}	349 ± 67^{a}
NT	226.7 ± 89.9^{b}	227.7 ± 92.5^{b}	4.60 ± 0.90^{b}	203 ± 85^{b}

Date shown are the mean ± standard deviations. Superscript lettering a and b indicate the significant differences between participants. DR-TB: drug resistant tuberculosis; DS-TB: drug sensitive tuberculosis; NT: Normal tissues.

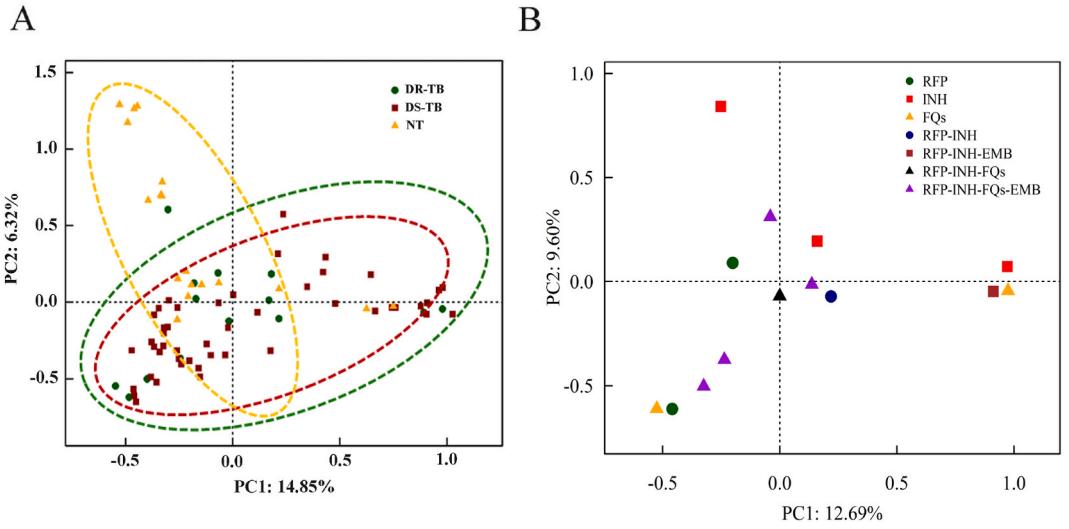

Fig. 3. Principal coordinate analysis (PCoA) based on Bray-Curtis dissimilarity in OTU level displaying the bacterial variations for (A) all samples and (B) DR-TB lesions. DR-TB: drug resistant tuberculosis; DS-TB: drug sensitive tuberculosis; NT: Normal tissues. INH: isoniazide, RFP: rifampicin, FQs: fluoroquinolone, EMB: ethambutol.

Interestingly, there was no striking separation observed in the bacterial community between DS-TB and DR-TB groups (ANOSIM, $R = 0.069$, $p = 0.173$). These findings suggest that the bacterial composition structures in TB lesions were not associated with the drug susceptibility.

To further investigate whether the bacteriome were associated with different drug-resistant phenotypes, we employed PCoA to visualize the characteristics of bacterial structures among DR-TB lesions (Fig. 3B). The Bacterial community in lesions of different drug-resistant phenotypes seemed to separate from each other. However, the significance of this differences in bacterial structures still needed a larger sample size to confirm.

3.2. Bacterial functions predicted in DR-TB, DS-TB and NT samples

Bacterial functions were predicted using the PICRUSt2 platform based on the 16S rRNA sequencing data generated from lung tissues. The cluster of orthologous groups (COG) functional categories mainly included [A] RNA processing and modification, [B] chromatin structure and dynamics, [C] energy production and conversion, etc (Table 3). These functions play crucial roles in sustaining the stability of bacterial communities. COG functions between DR-TB and DS-TB showed no significant differences. Compared to NT samples, all COG functions were enriched in TB lesions, with several related to substance metabolism significantly enriched in both DR-TB and DS-TB lesions. [J] Translation, ribosomal structure and biogenesis was the most enriched COG function in TB lesions, indicating increased metabolic activity of the lung bacteriome.

To further elucidate the potential biological functions of the bacteriomes, we also predicted Kyto Encyclopedia of Genes and Genomes (KEGG) enzymes. Compared to NT samples, 657 KEGG enzymes were significantly enriched in TB lesions and the top two enriched enzymes were prephenate dehydrogenase (EC:1.3.1.12, $p < 0.001$) and holo-[acyl-carrier-protein] synthase (EC:2.7.8.7, $p < 0.001$) (Fig. 4A). Additionally, several other KEGG enzymes were also enriched in TB lesions, including 16S rRNA methyltransferase (EC:2.1.1.198, EC:2.1.1.227), aminoacyl-tRNA hydrolase (EC:3.1.1.29), nitrite reductase (EC:1.7.2.1) and nitrate reductase (EC:1.7.1.2). Enriched KEGG enzymes were also observed in NT samples, such as cutinase (EC:3.1.1.74), 2′-hydroxybiphenyl-2-sulfinate desulfinase (EC:3.13.1.3), D-arabinitol dehydrogenase (EC:1.1.1.287), Aureolysin (EC:3.4.24.29), Cyanophycinase (EC:3.4.15.6) and fatty acid amide hydrolase (EC:3.5.1.99). Notably, the pattern of volcano plots for TB vs. NT was quite similar to that for DS-TB vs. NT, likely due to the larger proportion of DS-TB samples (Fig. 4B). Compared to DR-TB lesions, several bacterial KEGG enzymes were enriched in NT samples, including D-arabinitol dehydrogenase (EC:1.1.1.287), 2′-hydrpxybiphenyl-2-sulfinate desulfinase (EC:3.13.1.3), aureolysin (EC:3.4.24.29) and fatty acid amide hydrolase (EC:3.5.1.99) (Fig. 4C). One hundred and twenty-six KEGG enzymes were significantly enriched in DR-TB lesions compared to DS-TB lesions (Fig. 4D) and the top two enriched enzymes were quaternary-amine-transporting ATPase (EC:3.6.3.32, $p = 0.002$) and methylglyoxal synthase (EC:4.2.3.3, $p = 0.003$). Some enzymes were also enriched in DS-TB lesions, including Homoserine O-succinyltransferase (EC:2.3.1.46), 2-dehydropantoate 2-reductase (EC:1.1.1.169) and NAD(+) synthase (EC:6.3.1.5) (Fig. 4D). These results collectively indicate that MTB infection can modulate pulmonary bacterial functions, and some bacterial KEGG enzymes in TB lesions are associated with drug susceptibility.

4. Discussion

To our knowledge, most studies have investigated lung bacteriomes of drug-resistant pulmonary TB patients using sputum, BAL and throat swabs [15–19]. Certain bacterial taxa found in sputum can even serve as biomarker for chronicity in RIF- and multidrug-resistant TB patients [17]. However, sputum, BLA and throat swabs are all susceptible to contamination by environmental organisms, and the bacteriome in these samples cannot precisely represent the entire population in the lower respiratory tract,

Table 3
The differences of COG functional categories among DR-TB, DS-TB and NT samples by Wilcoxon rank sum test.

Category	Description	DR-TB vs DS-TB	DR-TB vs NT	DS-TB vs NT
A	RNA processing and modification	0.670[a]	0.069	0.027
B	Chromatin structure and dynamics	0.509	0.186	0.122
C	Energy production and conversion	0.262	0.054	0.033 *
D	Cell cycle control, cell division, chromosome partitioning	0.237	0.026 *	0.008 **
E	Amino acid transport and metabolism	0.062	0.066	0.104
F	Nucleotide transport and metabolism	0.186	0.010 *	0.002 **
G	Carbohydrate transport and metabolism	0.060	0.023 *	0.011 *
H	Coenzyme transport and metabolism	0.250	0.017 *	0.005 **
I	Lipid transport and metabolism	0.564	0.014 *	0.003 **
J	Translation, ribosomal structure and biogenesis	0.286	0.008 **	<0.001 ***
K	Transcription	0.103	0.036 *	0.030 *
L	Replication, recombination and repair	0.327	0.043 *	0.012 *
M	Cell wall/membrane/envelope biogenesis	0.204	0.041 *	0.019 *
N	Cell motility	0.114	0.144	0.352
O	Posttranslational modification, protein turn over,	0.406	0.026 *	0.006 **
P	chaperones	0.094	0.074	0.094
Q	Inorganic ion transport and metabolism	0.570	0.059	0.037 *
R	Second metabolites biosynthesis, transport and catabolism	0.278	0.054	0.035 *
S	General function prediction only	0.310	0.067	0.043 *
T	Function unknown	0.184	0.062	0.074
U	Signal transduction mechanisms	0.338	0.293	0.355
V	Intracellular trafficking, secretion, and vesicular transport	0.590	0.032 *	0.012 *
W	Defense mechanisms	0.432	0.295	0.363
X	Extracellular structures	0.749	0.559	0.569
Z	Mobilome: prophages, transposons	0.618	0.005 **	0.004 **
	Cytoskeleton			

*: $p<0.05$; **: $p<0.01$; ***: $p<0.001$. DR-TB: drug resistant tuberculosis; DS-TB: drug sensitive tuberculosis; NT: Normal tissues
[a] : p value of Wilcoxon rank sum test.

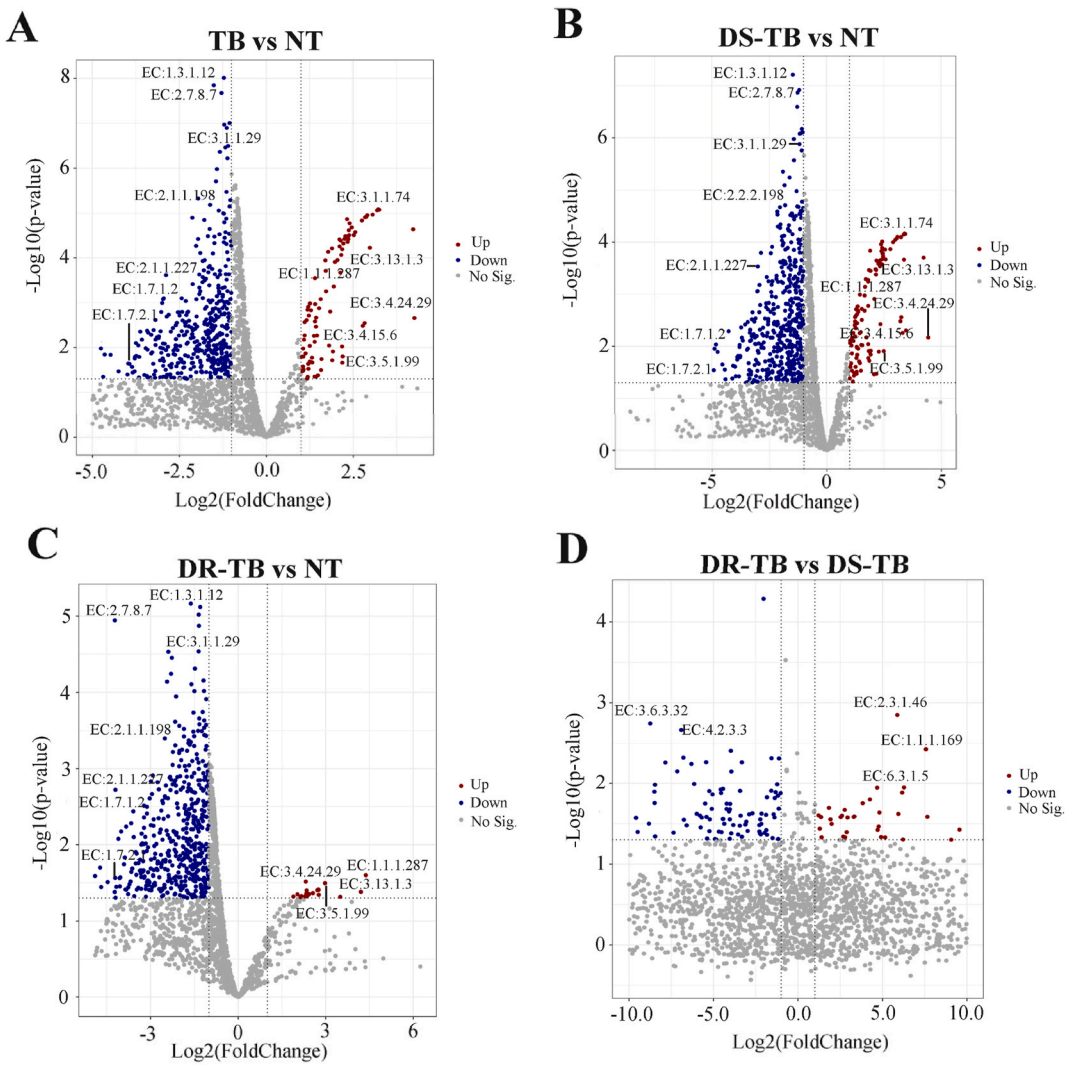

Fig. 4. (A) Volcano plot showing the bacterial KEGG that are up/down regulated in TB lesions compared to NT samples. (B) Volcano plot showing the bacterial KEGG that are up/down regulated in DS-TB compared to NT samples. (C) Volcano plot showing the bacterial KEGG that are up/down regulated in DR-TB compared to NT samples. (D) Volcano plot showing the bacterial KEGG that are up/down regulated DR-TB compared to DS-TB. DR-TB: drug resistant tuberculosis; DS-TB: drug sensitive tuberculosis; NT: Normal tissues.

particularly within TB lesions. The physiological and biochemical conditions within TB lesions undergo significant changes due to MTB infection, resulting in an entirely new microenvironment for bacteriomes. This study initially focused on characterizing bacteriomes within TB lesions, and investigated the association between lung bacteriomes and drug susceptibility using normal lung tissues as the bacterial baseline.

The bacterial communities within TB lesions deviated from the baseline, reflecting the impact of both MTB infection and anti-tuberculosis treatment on the pulmonary bacteriome. Among TB lesions, the dominant phyla, ranked by relative abundance from high to low, are *Proteobacteria*, *Actinobacteria*, *Bacteroidetes*, *Firmicutes* and *Fusobacteria*. Although the phylum categories remain consistent between TB lesions and sputum, their proportions varied slightly. TB sputum samples exhibit a different order: *Firmicutes*, *Proteobacteria*, *Bacteroidetes* and *Actinobacteria* [19]. Interestingly, the bacterial compositions, including α diversity and β diversity, in DS-TB sputum significantly overlap with those in DR-TB sputum [19], which aligns with our findings based on TB lesions. Bacterial profile of individual DR-TB sample was diverged from each other, and clustered together with DS-TB samples. The heterogeneity of individual bacterial was reported in the macaque model using lung lobe washes, which was consistent with our study [31]. Nevertheless, the indicator genera identified in DS-TB and DR-TB samples still suggested distinct micro-ecological environments within TB lesions. Given the small sample size, associations between bacterial compositions within DR-TB lesions and TB drug resistant phenotypes cannot be confirmed. Anti-tuberculosis drugs target not only MTB bacilli but also affect inherent organisms within lesions. Different antibiotics can rapidly and thoroughly alter the bacterial composition, resulting in varying profiles [24]. Lung bacteriomes exhibit minimal variation among individuals [31,32], which makes it difficult to observe bacterial differences among various

drug-resistant types.

Using 16S rRNA data generated from TB lesions and NT samples, we predicted bacterial metabolic activities on the PICRUSt2 platform. Notably, several COG functional categories responsible for metabolic activities presented higher abundance in TB lesions compared to that of NT samples, suggesting increased biological activities of lung bacteriome after MTB infection. The [J] translation, ribosomal structure and biogenesis was the most significantly enriched COG function in TB lesions, and it played a vital role in sustaining bacterial metabolic function and growth.

KEGG analysis highlights distinct bacterial functions related to pulmonary TB. Nitric oxide generated from nitrite or nitrate reduction serves as an electron donor for anaerobic bacteria. In TB lesions, both nitrite and nitrate reductase are significantly enriched, indicating a hypoxia condition. The hypoxia is likely linked to damaged vascularization within necrotic granulomas due to antituberculosis immune responses, and various animal infection models also exhibit hypoxia in TB lesions [33]. Another intriguing finding is the exogenously acquired 16S rRNA methyltransferase within TB lesions, which confers high-level aminoglycoside resistance. This enzyme is widely distributed among taxonomically distinct organisms [34]. Pathogens use this epigenetic mechanism to develop resistance against certain drug molecules and it can be used as novel drug target against tuberculosis [35]. In NT samples, the enriched D-arabinitol dehydrogenase plays a crucial role in the chemical synthesis of rare chiral sugars and sugar derivatives [36]. These rare sugars participate in host physiological functions and have a protective effect on the innate immune system, contributing to the maintenance of lung health [37].

Within DR-TB lesions, the enrichment of bacterial ATPase plays a crucial role in mediating protein phosphorylation. This modification facilitates cross-talks among proteins associated with sensing external pressure and bacterial complex signal transduction [38]. Methylglyoxal, a toxic secretory electrophile produced by the action of methylglyoxal synthase in many bacteria [39], is also enriched in DR-TB lesions. The enriched methylglyoxal synthase may suggest robust resistance of inherent lung bacteriomes against invasive MTB bacilli. In DS-TB lesions, the homoserine O-succinyltransferase was enriched, which was a critical enzyme involving in methionine biosynthesis [40]. Methionine provides methyl groups for lipids, proteins, nucleic acids and alkaloids. It participates in the regulation of cell division, differentiation, apoptosis and homeostasis [41]. Overall, the distinct enrichment of bacterial enzymes in DR-TB and DS-TB lesions suggest that pulmonary bacterial activities are partly associated with the drug susceptibility of MTB bacilli.

This study provides vital bacterial information associated with drug susceptibility of pulmonary tuberculosis using TB lesions. One disadvantage of this retrospective study is the disequilibrium sample numbers of DR-TB and DS-TB samples, which can generate some bacterial deviations.

5. Conclusion

The bacterial communities in pulmonary DR-TB and DS-TB lesions showed no significant differences, while indicator genera suggested distinctive ecological environments between them. No significant correlation between bacterial communities and drug resistance types was observed due to the small sample size. Most COG functions were enriched in TB lesions compared to NT samples, and the most significant one was [J] translation, ribosomal structure and biogenesis. Enriched bacterial functions observed in DR-TB and DS-TB played vital role in sustaining the physiological functions of pulmonary micro-niches. This study innovatively bridges the gap between tuberculosis drug susceptibility and pulmonary bacteriomes using lung tissues, providing essential insights for developing novel strategies in tuberculous prevention and treatment.

Ethical approval

This study was approved by the ethical and institutional review boards for human investigation at Beijing Chest Hospital, Capital Medical University (Number: (2023)-review opinion-scientific research -(No.36)).

Data availability

16S rDNA raw data were deposited at Sequence Read Archive (SRA) under BioProject accession number PRJNA853869.

CRediT authorship contribution statement

Weili Du: Writing – review & editing, Writing – original draft, Funding acquisition, Formal analysis, Data curation, Conceptualization. **Yingli Zhao:** Data curation. **Chen Zhang:** Data curation. **Li Zhang:** Data curation. **Lijuan Zhou:** Data curation. **Zuyu Sun:** Data curation. **Xiaojie Huang:** Data curation. **Nana Zhang:** Data curation. **Zichen Liu:** Data curation. **Kun Li:** Data curation. **Nanying Che:** Writing – review & editing, Supervision, Funding acquisition, Conceptualization.

Declaration of competing interest

All authors declare that they have no conflicts of interests.

Acknowledgements

This work was supported by grants from Beijing Hospitals Authority Youth Programme (QML20231603), the National Natural

Science Foundation of China, China (31900098, 82072381), Beijing Municipal Science and Technology Project (Z181100001918027, Z191100006619079), and Tongzhou High-level Technique Talents Program (YHLD2018006).

Appendix A. Supplementary data

Supplementary data to this article can be found online at https://doi.org/10.1016/j.heliyon.2024.e37583.

References

[1] A. Iacobino, L. Fattorini, F. Giannoni, Drug-resistant tuberculosis 2020: where we stand, Appl. Sci. 10 (2020) 2153, https://doi.org/10.3390/app10062153.
[2] X.S. Xiong, X.D. Zhang, J.W. Yan, T.T. Huang, Z.Z. Liu, Z.K. Li, L. Wang, F. Li, Identification of *Mycobacterium tuberculosis* resistance to common antibiotics: an overview of current methods and techniques, Infect. Drug Resist. 17 (2024) 1491–1506, https://doi.org/10.2147/IDR.S457308.
[3] World Health Organization, Global tuberculosis report (2023). http://www.who.int/tb/publications/global_report/en/.
[4] L. Wang, X.D. Zhang, J.W. Tang, Z.W. Ma, M. Usman, Q.H. Liu, C.Y. Wu, F. Li, Z.B. Zhu, B. Gu, Machine learning analysis of SERS fingerprinting for the rapid determination of *Mycobacterium tuberculosis* infection and drug resistance, Comput. Struct. Biotechnol. J. 20 (2022) 5364–5377, https://doi.org/10.1016/j.csbj.2022.09.031.
[5] M. Zignol, A.S. Dean, D. Falzon, W. Gemert, A. Wright, A. Deun, F. Portaels, A. Laszlo, M.A. Espinal, A. Pablos-Méndez, A. Bloom, M.A. Aziz, K. Weyer, E. Jaramillo, P. Nunn, K. Floyd, M.C. Raviglione, Twenty years of global surveillance of antituberculosis-drug resistance, N. Engl. J. Med. 375 (2016) 1081–1089, https://doi.org/10.1056/NEJMsr1512438.
[6] K.D. Mayer-Barber, D.L. Barber, Innate and adaptive cellular immune responses to *Mycobacterium tuberculosis* infection, Cold Spring Harb Perspect Med. 5 (2015) a018424, https://doi.org/10.1101/cshperspect.a018424.
[7] G. Mori, M. Morrison, A. Blumenthal, Microbiome-immune interactions in tuberculosis, PLoS Pathog. 17 (2021) e1009377, https://doi.org/10.1371/journal.ppat.1009377.
[8] V.L. Chen, D.L. Kasper, Interactions between the intestinal microbiota and innate lymphoid cells, Gut Microb. 5 (2014) 129–140, https://doi.org/10.4161/gmic.27289.
[9] J.O. Sekyere, N. Maningi, P.B. Fourie, *Mycobacterium tuberculosis*, antimicrobials, immunity, and lung-gut microbiota crosstalk: current updates and emerging advances, Ann. N. Y. Acad. Sci. 1467 (2020) 21–47, https://doi.org/10.1111/nyas.14300.
[10] C.C. Naidoo, G.R. Nyawo, I. Sulaiman, B.G. Wu, C.T. Turner, K. Bu, Z. Palmer, Y. Li, B.W.P. Reeve, S. Moodley, J.G. Jackson, J. Limberis, A.H. Diacon, P. D. Helden, J.C. Clemente, R.M. Warren, M. Noursadeghi, L.N. Segal, G. Theron, Anaerobe-enriched gut microbiota predicts pro-inflammatory responses in pulmonary tuberculosis, EBioMedicine 67 (2021) 103374, https://doi.org/10.1016/j.ebiom.2021.103374.
[11] F. Yang, Y. Yang, L. Chen, Z. Zhang, L. Liu, C. Zhang, Q. Mai, Y. Chen, Z. Chen, T. Lin, L. Chen, H. Guo, L. Zhou, H. Shen, X. Chen, L. Liu, G. Zhang, H. Liao, L. Zeng, G. Zeng, The gut microbiota mediates protective immunity against tuberculosis via modulation of lncRNA, Gut Microb. 14 (2022) 2029997, https://doi.org/10.1080/19490976.2022.2029997.
[12] J. Shi, G. Gao, Z. Yu, K. Wu, Y. Huang, L.P. Wu, Z. Wu, X. Ye, C. Qiu, X. Jiang, The relevance of host gut microbiome signature alterations on de novo fatty acids synthesis in patients with multi-drug resistant tuberculosis, Infect. Drug Resist. 15 (2022) 5589–5600, https://doi.org/10.2147/IDR.S372122.
[13] R.P. Dickson, J.R. Erb-Downward, G.B. Hufnagle, Towards an ecology of the lung: new conceptual models of pulmonary microbiology and pneumonia pathogenesis, Lancet Resp Med 2 (2014) 238–246, https://doi.org/10.1016/S2213-2600(14)70028-1.
[14] D. Nejman, I. Livyatan, G. Fuks, N. Gavert, Y. Zwang, L.T. Geller, A. Rotter-Maskowitz, R. Weiser, G. Mallel, E. Gigi, A. Meltser, G.M. Douglas, I. Kamer, V. Gopalakrishnan, T. Dadosh, S. Levin-Zaidman, S. Avnet, T. Atlan, Z.A. Cooper, R. Arora, A.P. Cogdill, M.A.W. Khan, G. Ologun, Y. Bussi, A. Weinberger, M. Lotan-Pompan, O. Golani, G. Perry, M. Rokah, K. Bahar-Shany, E.A. Rozeman, C.U. Blank, A. Ronai, R. Shaoul, A. Amit, T. Dorfman, R. Kremer, Z.R. Cohen, S. Harnof, T. Siegal, E. Yehuda-Shnaidman, E.N. Gal-Yam, H. Shapira, N. Baldini, M.G.I. Langille, A. Ben-Nun, B. Kaufman, A. Nissan, T. Golan, M. Dadiani, K. Levanon, J. Bar, S. Yust-Katz, I. Barshack, D.S. Peeper, D.J. Raz, E. Segal, J.A. Wargo, J. Sandbank, N. Shental, R. Straussman, The human tumor microbiome is composed of tumor type-specific intracellular bacteria, Science 368 (2020) 973–980, https://doi.org/10.1126/science.aay9189.
[15] P. Krishna, A. Jain, P.S. Bisen, Microbiome diversity in the sputum of patients with pulmonary tuberculosis, Eur. J. Clin. Microbiol. 35 (2016) 1205–1210, https://doi.org/10.1007/s10096-016-2654-4.
[16] N. Wiqoyah, N.M. Mertaniasih, W.T. Artama, S. Matsumoto, Microbiome in sputum as a potential biomarker of chronicity in pulmonary resistant to rifampicin-tuberculosis and multidrug-resistant-tuberculosis patients, Int J Mycobacteriol 10 (2021) 260–267, https://doi.org/10.4103/ijmy.ijmy_132_21.
[17] D. Lin, X. Wang, Y. Li, W. Wang, Y. Li, X. Yu, B. Lin, Y. Chen, C. Lei, X. Zhang, X. Zhang, J. Huang, B. Lin, W. Yang, J. Zhou, J. Zeng, X. Liu, Sputum microbiota as a potential diagnostic marker for multidrug-resistant tuberculosis, Int. J. Med. Sci. 18 (2021) 1935–1945, https://doi.org/10.7150/ijms.53492.
[18] M.R. Wood, E.A. Yu, S. Mehta, The human microbiome in the fight against tuberculosis, Am. J. Trop. Med. Hyg. 96 (6) (2017) 1274–1284, https://doi.org/10.4269/ajtmh.16-0581.
[19] F. Valdez-Palomares, M. Muñoz Torrico, B. Palacios-González, X. Soberón, E. Silva-Herzog, Altered microbial composition of drug-sensitive and drug-resistant TB patients compared with healthy volunteers, Microorganisms 9 (2021) 1762, https://doi.org/10.3390/microorganisms9081762.
[20] J.M. Baker, K.J. Hinkle, R.A. McDonald, C.A. Brown, N.R. Falkowski, G.B. Huffnagle, R.P. Dickson, Whole lung tissue is the preferred sampling method for amplicon-based characterization of murine lung microbiota, Microbiome 9 (2021) 99, https://doi.org/10.1186/s40168-021-01055-4.
[21] J.P. Sarathy, V. Dartois, Caseum: a niche for *Mycobacterium tuberculosis* drug-tolerant persisters, Clin. Microbiol. Rev. 33 (2020) e00159, https://doi.org/10.1128/CMR.00159-19, 19.
[22] L. Zhan, J. Wang, L. Wang, C. Qin, The correlation of drug resistance and virulence in *Mycobacterium tuberculosis*, Biosaf Health 2 (2024) 18–24, https://doi.org/10.1016/j.bsheal.2020.02.004.
[23] N.C. Howard, N.D. Marin, M. Ahmed, B.A. Rosa, J. Martin, M. Bambouskova, A. Sergushichev, E. Loginicheva, N. Kurepina, J. Rangel-Moreno, L. Chen, B. N. Kreiswirth, R.S. Klein, J. Balada-Llasat, J.B. Torrelles, G.K. Amarasinghe, M. Mitreva, M.N. Artyomov, F. Hsu, B. Mathema, S.A. Khader, *Mycobacterium tuberculosis* carrying a rifampicin drug resistance mutation reprograms macrophage metabolism through cell wall lipid changes, Nat Microbiol 3 (2018) 1099–1108, https://doi.org/10.1038/s41564-018-0245-0.
[24] S. Louca, M.F. Polz, F. Mazel, M.B.N. Albright, J.A. Huber, M.I. O'Connor, M. Ackermann, A.S. Hahn, D.S. Srivastava, S.A. Crowe, M. Doebeli, L.W. Parfrey, Function and functional redundancy in microbial systems, Nat Ecol Evol 2 (2018) 936–943, https://doi.org/10.1038/s41559-018-0519-1.
[25] G.M. Douglas, V.J. Mafei, J.R. Zaneveld, S.N. Yurgel, J.R. Brown, C.M. Taylor, C. Huttenhower, M.G.I. Langille, PICRUSt2 for prediction of metagenome functions, Nat. Biotechnol. 38 (2020) 685–688, https://doi.org/10.1038/s41587-020-0548-6.
[26] E.A. Eloe-Fadrosh, N.N. Ivanova, T. Woyke, N.C. Kyrpides, Metagenomics uncovers gaps in amplicon-based detection of microbial diversity, Nat Microbiol 1 (2016) 15032, https://doi.org/10.1038/nmicrobiol.2015.32.
[27] J.G. Caporason, J. Kuczynski, J. Stombaugh, K. Bittinger, F.D. Bushman, E.K. Costello, N. Fierer, A.G. Peña, J.K. Goodrich, J.I. Gordon, G.A. Huttley, S.T. Kelley, D. Knights, J.E. Koenig, R.E. Ley, C.A. Lozupone, D. McDonald, B.D. Muegge, M. Pirrung, J. Reeder, J.R. Sevinsky, P.J. Turnbaugh, W.A. Walters, J. Widmann, T. Yatsunenko, J. Zaneveld, R. Knight, QIIME allows analysis of high-throughput community sequencing data, Nat. Methods 7 (2010) 335–336, https://doi.org/10.1038/nmeth.f.303.

[28] R.C. Edgar, Search and clustering orders of magnitude faster than BLAST, Bioinformatics 26 (2010) 2460–2461, https://doi.org/10.1093/bioinformatics/btq461.
[29] J.A. Navas-Molina, J.M. Peralta-Sánchez, A. González, P.J. McMurdie, Y. VázquezBaeza, Z. Xu, L.K. Ursell, C. Lauber, H. Zhou, S.J. Song, J. Huntley, G. L. Ackermann, D. Berg-Lyons, S. Holmes, J.G. Caporaso, R. Knight, Advancing our understanding of the human microbiome using QIIME, Methods Enzymol. 531 (2013) 371–444, https://doi.org/10.1016/B978-0-12-407863-5.00019-8.
[30] D.J. Kahle, H. Wickham, ggmap: spatial visualization with ggplot2, R J 5 (2013) 144.
[31] A.M. Cadena, Y. Ma, T. Ding, M. Bryant, P. Maiello, A. Geber, P.L. Lin, J.L. Flynn, E. Ghedin, Profiling the airway in the macaque model of tuberculosis reveals variable microbial dysbiosis and alteration of community structure, Microbiome 6 (2018) 180, https://doi.org/10.1186/s40168-018-0560-y.
[32] A. Ekanayake, D. Madegedara, V. Chandrasekharan, D. Magana-Arachchi, Respiratory bacterial microbiota and individual bacterial variability in lung cancer and bronchiectasis patients, Indian J. Microbiol. 60 (2) (2020) 196–205, https://doi.org/10.1007/s12088-019-00850-w.
[33] J.P. Sarathy, V. Dartois, Caseum: a niche for *Mycobacterium tuberculosis* drug-tolerant persisters, Clin. Microbiol. Rev. 33 (2020) e00159, https://doi.org/10.1128/CMR.00159-19, 19.
[34] J.I. Wachino, Y. Doi, Y. Arakawa, Aminoglycoside resistance: updates with a focus on acquired 16S ribosomal RNA methyltransferases, Infect Dis Clin North Am 34 (2020) 887–902, https://doi.org/10.1016/j.idc.2020.06.002.
[35] M.R. Salaikumaran, V.P. Badiger, V.L.S.P. Burra, 16S rRNA methyltransferases as novel drug targets against tuberculosis, Protein J. 41 (1) (2022) 97–130, https://doi.org/10.1007/s10930-021-10029-2.
[36] V. Kallnik, C. Schulz, P. Schweiger, U. Deppenmeier, Properties of recombinant strep-tagged and untagged hyperthermophilic D-arabitol dehydrogenase from *Thermotoga maritima*, Appl. Microbiol. Biotechnol. 90 (2011) 1285–1293, https://doi.org/10.1007/s00253-011-3187-5.
[37] A. Murata, K. Sekiya, Y. Watanabe, F. Yamaguchi, N. Hatano, K. Izumori, M. Tokuda, A novel inhibitory effect of D-allose on production of reactive oxygen species from neutrophils, J. Biosci. Bioeng. 96 (2003) 89–91, https://doi.org/10.1016/s1389-1723(03)90104-6.
[38] M.J. Suskiewicz, T. Clausen, Chemical biology interrogates protein arginine phosphorylation, Cell Chem. Biol. 23 (2016) 888–890, https://doi.org/10.1016/j.chembiol.2016.08.003.
[39] G.P. Ferguson, S. Tötemeyer, M.J. MacLean, I.R. Booth, Methylglyoxal production in bacteria: suicide or survival? Arch. Microbiol. 170 (1998) 209–218, https://doi.org/10.1007/s002030050635.
[40] H.Y. Sagong, D. Lee, I.K. Kim, K.J. Kim, Rational engineering of homoserine O-Succinyltransferase from *Escherichia coli* for reduced feedback inhibition by methionine, J. Agric. Food Chem. 70 (2022) 1571–1578, https://doi.org/10.1021/acs.jafc.1c07211.
[41] M. Sauter, B. Moffatt, M.C. Saechao, R. Hell, M. Wirtz, Methionine salvage and S-adenosylmethionine: essential links between sulfur, ethylene and polyamine biosynthesis, Biochem. J. 451 (2013) 145–154, https://doi.org/10.1042/BJ20121744.